Highly Efficient Light Helicity Detection of Enantiomers by Chiral Metal–Organic Framework Thin Films

Yi-Bo Tian, Koichi Tanaka, Li-Mei Chang, Christof Wöll,* Zhi-Gang Gu,* and Jian Zhang

ABSTRACT: The potential of chiral metal–organic frameworks (MOFs) for circularly polarized (CP) optics has been largely unexplored. Herein, we have successfully deposited monolithic and highly oriented chiral MOF thin films prepared by a layer-by-layer method (referred to as surface-coordinated MOF thin films, SURMOF) to fabricate CP photodetection devices and distinguish enantiomers. The helicity-sensitive absorption induced by a pair of enantiopure oriented SURMOF was found to be excellent, with an anisotropy factor reaching 0.41. Moreover, the chiral SURMOFs exhibited a pronounced difference in the uptake of the L- and D-tryptophane nantiomers. To demonstrate the potential of these novel MOF thin films for chirality analysis, we fabricated a portable sensor device that allows for chiral recognition by monitoring the photocurrent signals. Our findings not only introduce a new concept of using chiral building blocks for realizing direct CP photodetectors but also provide a blueprint for novel devices in chiral optics.

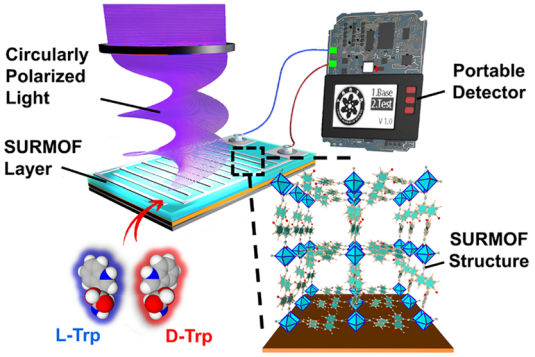

KEYWORDS: *Chiral metal–organic framework, Thin film, Circularly polarized photodetector, Enantiomer recognition*

Circular polarization is an inherent and crucial property of photons and thus provides the basis for many optical technologies, including data storage,[1] drug screening,[2] security surveillance,[3] remote sensing,[4] and optical quantum computing.[5,6] While some animal species possess visual systems that allow them to distinguish between left- and right-handed circularly polarized (CP) light,[7] the fabrication of artificial devices for efficient helicity detection still represents a major technological challenge. Most commercial CP photodetectors use inorganic semiconductor photodetectors, such as Ge and InGaAs,[8] which are insensitive to photon handedness, necessitating the use of a linear polarizer and a quarter-wave plate. However, this requirement for additional optical elements severely restricts the overall performance of these systems, leading to significant losses in sensitivity and resolution.[9] Therefore, direct CP photodetectors without additional optical elements thus have intrinsic advantages over indirect strategies. The simplification of CP light detectors becomes mandatory in the context of large-scale integration and flexible optoelectronics since the bulky wave plates limit the minimum size of detectors sensitive to helicity.[10]

The most straightforward way for realizing direct CP photodetectors involves utilizing chiral materials with optical absorption.[10] In recent years, researchers have explored various types of photoactive chiral materials, which eliminate the need for additional optical elements to differentiate left-handed CP light (LCP) from right-handed CP light (RCP).[11] In 2013, Campbell et al. reported the first enantiomeric helicene organic semiconductor (OSC) transistor for CP photodetection.[12] Following this demonstration, several other studies have used chiral molecules as the responsive layer for direct CP photodetectors.[13−15] Besides organic compounds, chiral hybrid materials comprising inorganic and organic constituents have attracted significant interest since synergistic effects can lead to an increase in their performance. Indeed, the fusion of organic and inorganic components, resulting in materials with diverse structures and tunable functionalities, has contributed to a significant advancement in the field of chiral heterostructures[16] and chiral perovskites.[17−19]

In this context, metal–organic frameworks (MOFs) exhibit a number of unique, very attractive properties. MOFs are a type of crystalline porous organic–inorganic hybrid materials, constructed from metal nodes and organic linkers, which possess large surface areas, highly ordered pore structure, high stability, pronounced extensibility, and adjustable functionality.[20,21] These materials have been extensively investigated in fundamental research and have demonstrated diverse applications in fields such as adsorption/separation,[22] catalysis,[23] nonlinear optics,[24] and drug delivery.[25] Recently, MOFs have seen a rapid expansion for optoelectronic applications, given

Scheme 1. Schematic Diagram of the Fabrication Process of Chiral SURMOF-Based Photodetector

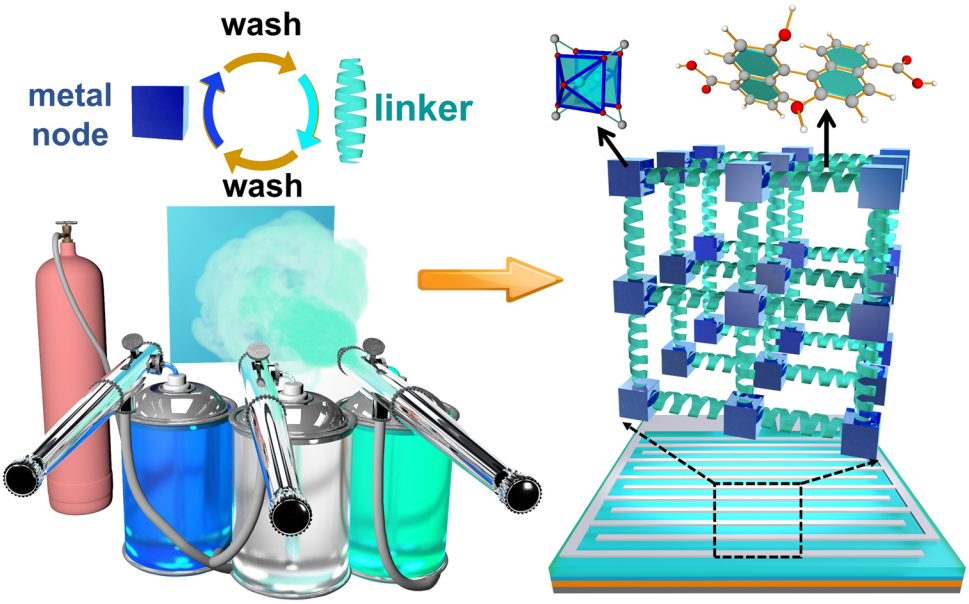

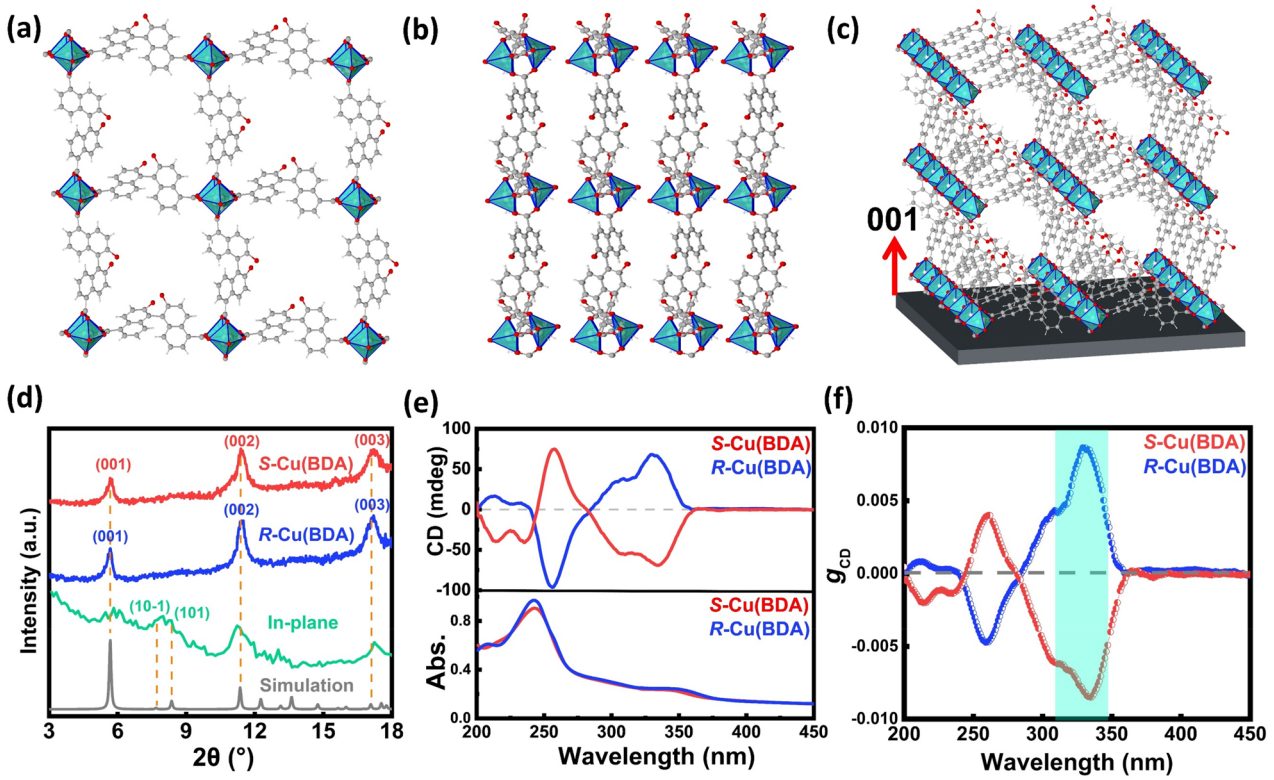

Figure 1. 2D chiral *R*-Cu(BDA) structural framework: (a) front view and (b) side view. (c) Schematic diagram of the growth of *R*-Cu(BDA) SURMOFs on the substrate along the [100] orientation. (d) Out-of-plane and in-plane XRD patterns of *R*- and *S*-Cu(BDA) SURMOF. (e) CD and absorbance spectra of *R*- and *S*-Cu(BDA) SURMOFs, respectively. (f) g_{CD} spectra of *R*- and *S*-Cu(BDA) SURMOFs.

their reticular, highly customizable nature, which allows them to combine high functionality with straightforward processing.[26−28] However, for many applications, the standard form of MOFs, powders, are not well suited because of unwanted scattering effects from the MOFs particles. As a result, monolithic thin films with low defect density are required for a reliable characterization of optical parameters and for the integration into devices.[29]

In recent years, a number of approaches to fabricating high optical quality MOF thin films have been presented, allowing, e.g., for the fabrication of photodetectors,[30] gas sensors,[31] field effect transistors (FETs),[32] solar cells,[33] nonlinear optics,[34] and so on. In this context, MOF thin films prepared by the liquid-phase epitaxial (LPE) layer-by-layer (LBL) growth method (referred to as surface-coordinated MOF thin films, SURMOF for short) have been demonstrated to provide an excellent basis for optoelectronic devices. Unique advantages of

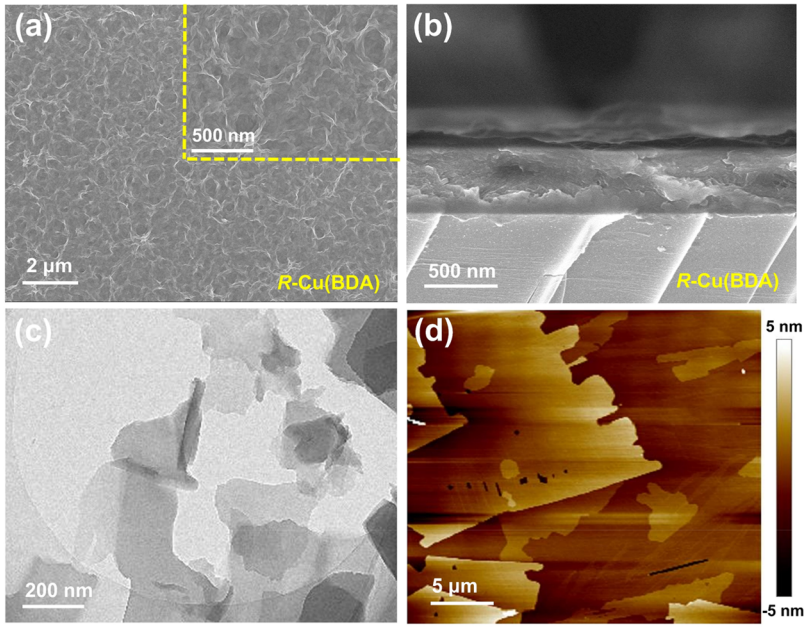

Figure 2. Surface SEM (a) and cross-sectional SEM (b) of the *R*-Cu(BDA) SURMOF. (c) and (d) TEM and AFM pictures of particles scratched from SURMOF.

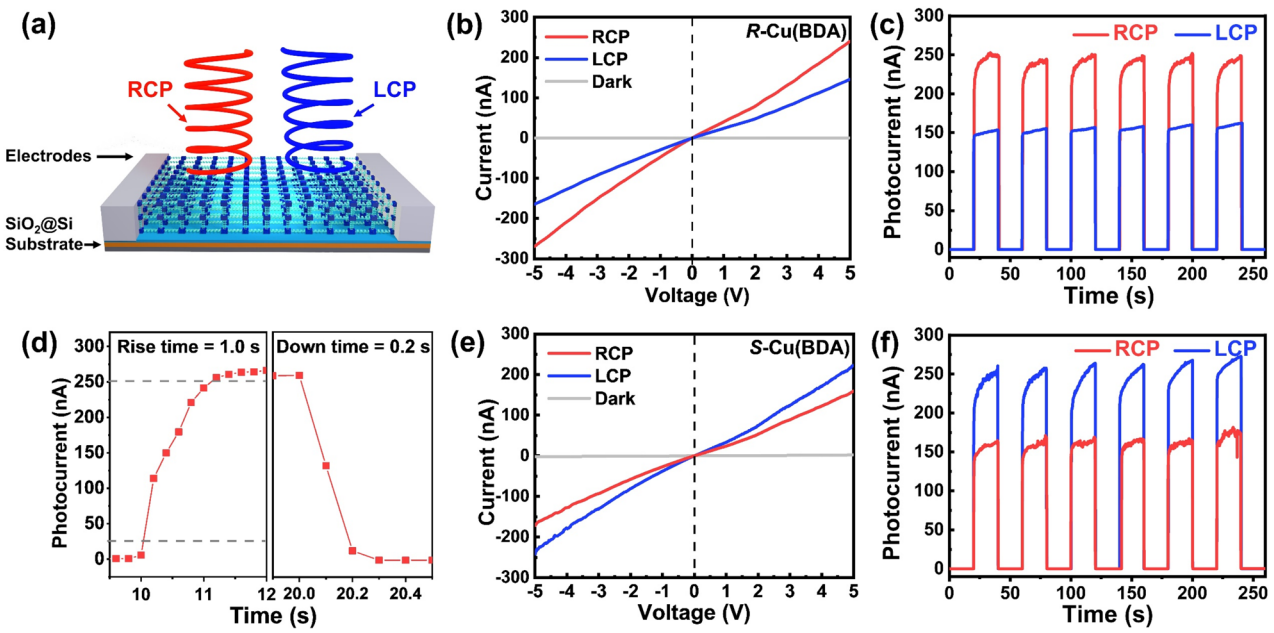

Figure 3. (a) Schematic diagram of circularly polarized photodetection for chiral SURMOFs based device. (b) Light dependent *I*−*V* curves of *R*-Cu(BDA) SURMOF under different 330 nm CP light from 5 to −5 V. (c) Time-resolved photocurrent as a function of illumination wavelength at 5 V bias voltage. (d) The rise/fall times curves for chiral SURMOFs are illuminated with ultraviolet light at 5 V bias voltage. (e) Light dependent *I*−*V* curves of *S*-Cu(BDA) SURMOFs. (f) Time-resolved photocurrent function under 330 nm illumination.

SURMOF are their strong adhesion to the substrate surface, controllable orientation, tunable thickness, low surface roughness. and monolithic structure.[35−37] Compared to other chiral materials, the small amount of chiral MOFs reported so far has limited the reports on applications of chiral MOFs. Because of the special procedures required for their fabrication, particularly the application on chiral MOF-based thin film devices is still in an early stage.[38,39] There is only one study to date that has demonstrated a minor anisotropy factor of 4.3×10^{-4} for light helicity detection, which is subject to its small chiral differential absorbance.[40,41] As a parallel research endeavor, chiral MOFs with a substantially larger anisotropy factor are required for competitive applications, and utilizing the chiral MOF nanopores for CP photodetection of enantiomers is still of great significance. Moreover, their ordered and porous nature allows chiral MOFs to be utilized to create highly sensitive detectors for different types of enantiomers. Such chiral sensors show huge potential applications in pharmaceutical synthesis, biological engineering, and toxicological testing.

Herein, we provide the fabrication of a chiral SURMOF with high optical sensitivity able to directly, without additional

optical devices, the helicity of incident light. We utilized a pair of enantiomeric linkers used in previous work for the fabrication of bulk (powder) MOFs, *R*- and *S*-Cu(BDA) (BDA = 2,2-dihydroxy-1,1-binaphthalene-5,5-dicarboxylic acid). As shown in Scheme 1, highly oriented chiral SURMOF was grown on solid substrates by using an LPE LBL spray platform (a system in which an aerosol is produced by expanding solutions of the reactants through a small nozzle). The precursor solution carried by the gas flow was coated on the substrate in a very homogeneous fashion. In the preparation process, the functionalized substrates were sequentially sprayed with cupric nitrate and an *R*/*S*-H_2BDA solution. After each deposition step, the sample underwent an ethanol wash to eliminate remaining unreacted reactants. Unless otherwise specified, the *R*- and *S*-Cu(BDA) SURMOFs were grown by using a total of 30 cycles and were grown on SiO_2/Si substrates. For additional information, please consult the Supporting Information section.

First, a thorough characterization of the SURMOF samples was carried out. The structure of the Cu(BDA) SURMOF from different directions is shown in Figure 1a and b. In this structure of *R*-Cu(BDA), each Cu(II) ion is coordinated by four carboxylate oxygen atoms of *R*-BDA ligand and each pair of Cu(II) ions is bridged by four carboxylate groups to form 2D square grid coordination networks with a Cu−Cu twisted paddle wheels structure.[42] The out-of-plane XRD data (see Figure 1d) revealed sharp peaks at 5.68°, 11.36°, and 17.12°, which are assigned to the (100), (200), and (300) peaks of the *R*-Cu(BDA) MOF, demonstrating the highly oriented nature of the SURMOF.[43] In the out-of-plane XRD diffraction patterns, only peaks along the (001) crystallographic direction can be seen, demonstrating a highly preferential growth of the

Scheme 2. Schematic Diagram of Enantiomers Detector[a]

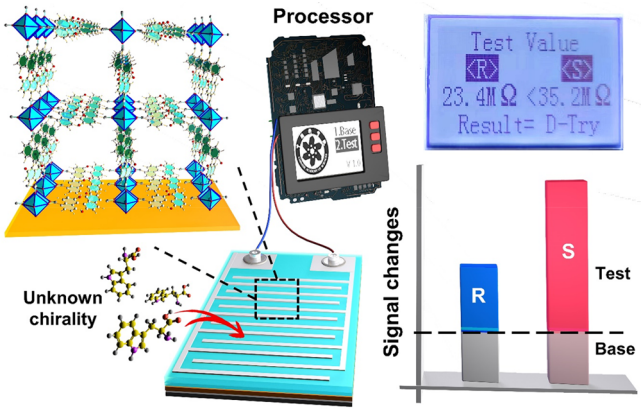

[a]The signal changes were analyzed by processor.

MOF thin film only along the [001] crystallographic orientation. The in-plane XRD patterns, which allowed us to determine the lattice plane spacing perpendicular to the substrate, revealed additional peaks around 7.65°and 8.35°. The out-of-plane XRD patterns combined with in-plane XRD patterns provided the complete structural information about the crystalline thin films and were fully consistent with the XRD data reported for the corresponding bulk material.[42] We therefore conclude that the SURMOF reported here exhibit the same structure as the bulk material. The 2D square grids are stacked perpendicular to the substrate to yield a monolithic thin film (Figure 1c). Note the similarity of these patterns to those reported previously for the SURMOF-2 reticular series of MOF thin films.[44] The compact 2D layered structure leads to an efficient coupling of adjacent chromophores, which is beneficial for the transport of charges.[45]

Due to the chromophoric nature of the BDA-linkers, the SURMOFs exhibit strong absorption in the near-ultraviolet. Additionally, the chiral nature of the linkers causes pronounced circular dichroism (CD) signals. As expected, the CD signals for the *R*-Cu(BDA) occur at the same wavelength as those for the *S*-Cu(BDA), but with opposite signs; see Figure 1e. From the CD and UV−vis spectra, the anisotropy factor g_{CD} was obtained (calculated as CD/(32980 × absorbances));[10] see Figure 1f. The UV−vis absorbance and CD spectra of the enantiopure ligand are shown in Figures S2 and S3. The solvated organic H_2BDA ligand without a regular topological arrangement in a crystalline framework did not exhibit a strong CD signal between 320 and 340 nm. The distinct CD signals of the SURMOFs are located around their characteristic absorption peaks. This work mainly focuses on the wavelengths of 320−340 nm. The intrinsic chirality of *R*- and *S*-Cu(BDA) in this range will readily induce some interesting chiral-electrical and chiral-optical properties, leading to promising CP photoelectric conversion.

The overall morphology of the deposited SURMOFs over larger scales is crucial for large-area preparation and the performance stability of photodetectors. The scanning electron microscope (SEM) images recorded for different sections of the SURMOFs (Figure 2a) revealed the presence of monolithic thin films with a residual roughness of about 50 nm. The thickness of the MOF thin films amounted to about 600 nm (for 30 deposition cycles; Figure 2b). Please note that each cycle of layer-by-layer deposition results in multiple lattice layers rather than just one lattice layer. The number of layers grown in a single cycle depends on the concentrations of the precursor solutions. For the investigation with transmission electron microscopy (TEM), a small fraction was scraped from the film and dispersed by ultrasonication (Figure 2c). The atomic force microscope (AFM) data allowed the identification of a clear 2D layer structure (Figure 2d).

In the next step, photodetectors were fabricated from chiral Cu(BDA) SURMOFs by connecting two probes to the MOFs thin films (Figure 3a). The characterization was carried out using a commercial semiconductor analysis system. A more detailed description of the specific experimental conditions and methods is provided in the Supporting Information. As shown in Figure 3b, the SURMOF-based device shows a clear and strong sensitivity to the handedness of the incident 330 nm CP light from 5 to −5 V. Due to the devices being assembled by the thin, polycrystalline SURMOFs with nanosheet structure, the *I*−*V* curves appeared as a very nonideal linear phenomenon. The dark current is nearly negligible, but the external illumination results in the creation of charge carriers, resulting in a fairly high photocurrent when applying an external bias voltage. For *R*-Cu(BDA), the photocurrent obtained for RCP light illumination was significantly larger (nearly 42%) than that achieved for LCP light, as demonstrated by the photocurrents recorded as a function of time while switching between the two different polarizations (Figure 3c). As illustrated in Figure S4, the long-term stability of the photodetectors under 330 nm was relatively high. The measured 10−90% rise and decay times were 1.0 and 0.2 s (Figure 3d). The signal response of the *S*-Cu(BDA) based

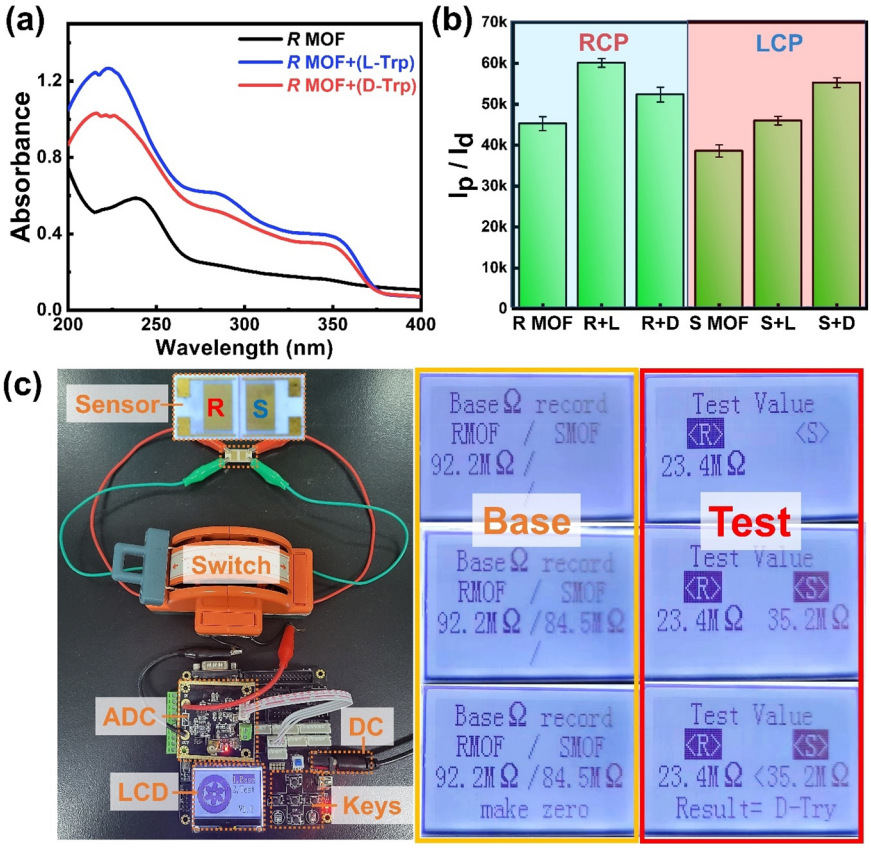

Figure 4. "*R* MOF" and "*S* MOF" are denoted as *R*-Cu(BDA) and *S*-Cu(BDA) in this figure, respectively. (a) UV curves of *R*-Cu(BDA) SURMOF after soaking with different solutions of L-and D-Trp enantiomers, respectively. (Tested with thin film samples on quartz substrates.) (b) On/off ratio of CP photodetector based on *R*- and *S*-Cu(BDA) SURMOF with opposite chiral tryptophan. (c) Rendering of the detector (development version) and LCD screen display of important steps (analog to digital converter, ADC; Liquid crystal display, LCD; Direct current, DC.).

device to the handedness of CP light (Figure 3e,f) was opposite that of *R*-Cu(BDA).

The key point of merit for light helicity detection is the photocurrent anisotropy factor g_{Iph}, which is defined by $g_{Iph} = 2(I_L - I_R)/(I_L + I_R)$, where I_R and I_L represent the photocurrent under RCP and LCP illumination, respectively. The g_{Iph} value of 330 nm was determined to be 0.41 for *R*-Cu(BDA) and 0.40 for *S*-Cu(BDA), indicating a significant improvement in CP photodetection compared with previously reported MOF materials. In fact, these values are highly competitive compared to those reported for CP photodetectors made from other materials (Table S1). Photoresponsivity (R_λ) and detectivity (D^*) of the device can be estimated by the equations, $R_\lambda = I_{ph}/PS$ and $D^* = R_\lambda/(2eI_{dark}/S)^{1/2}$ (I_{ph} is the photocurrent, P is the irradiance power density, S is the effective illuminated area, e is the electronic charge, and I_{dark} is dark current).[46] The responsivity and detectivity of *R*-Cu(BDA) were calculated as $R_\lambda = 198\ \mu A\ W^{-1}$ and $D^* = 5.02 \times 10^9$ Jones.

The potential uses of Cu(BDA) SURMOFs extend beyond the detection of CP light. Our porous coordination polymers are made from chiral ligands, thus presenting a unique chiral spatial selectivity realized through weak interactions with the chiral ligands (e.g., Coulomb force and hydrogen bonding).[47] The conventional techniques for chiral recognition involve the use of chromatography and subsequent analysis using circular polarization spectroscopy.[48] These methods are highly precise and exhibit exceptional performance. However, the equipment needed for these techniques is sizable and expensive. In various applications, such as the pharmaceutical industry, there is a need for rapid determination of chiral molecular configuration, calling for portable devices.[49] Tryptophan, an essential, naturally occurring chiral amino acid, possesses pharmacologically relevant properties, such as the ability to modulate circadian rhythms and improve sleep quality, making it a crucial component in drug development.[50] To this end, we selected L- and D-tryptophan (abbreviated as Trp) as target enantiomers by utilizing the different interactions of chiral pores of SURMOFs to design a rapid prototype of a tryptophan detector. The SURMOF constructed from chiral ligands possesses a large number of chiral pores to accommodate guest molecules. So, the chiral environment provided by Cu(BDA) SURMOF is of paramount importance due to the potential of enantiomers having a stereospecific interaction to build weak noncovalent bonds with that chiral environment. As a result, the binding of the chiral guests in the host pores, resulting from stereospecific interactions to build weak, noncovalent bonds with the chiral pore walls,[51] will be strongly different between enantiomers. Scheme 2 provides a clear overview of the experimental content of CP photodetectors of enantiomers.

We fabricated CP photodetectors based on the *R*-Cu(BDA) SURMOF and immersed them into different solutions of L- and D-Trp enantiomers. The specific procedures of this operation are described in the Supporting Information. As depicted in Figure 4a, the UV absorption of *R*-Cu(BDA)

SURMOF showed a pronounced increase after immersion in the tryptophan solution. According to Lambert−Beer's law, the quantity of light absorbed is proportional to the amount of substance.[52] Therefore, *R*-Cu(BDA) SURMOF absorbed more L-Trp than D-Trp under an equal process. The same experimental procedure gave opposite results for the *S*-Cu(BDA) SURMOF, as shown in Figure S5. To demonstrate the different binding affinities of enantiomers inside the pores of chiral Cu(BDA), we have carried out a theoretical inference. The binding energy, an important indicator to measure the binding affinities, is defined as the smallest amount of energy required to remove a particle from a system of particles or to disassemble a system of particles into individual parts.[53,54] AutoDock is a suite of automated docking tools designed to predict how small molecules, such as substance or drug candidates, bind to a receptor of a known framework structure. With the help of the Lamarckian Genetic Algorithm (LGA) provided by the AutoDock 4.2.6 software,[55] the binding energies between the enantiomer guest and Cu(BDA) host framework were simulated that the *R*-Cu(BDA) MOF have larger binding energy for L-Try than D-Try by 0.5 eV. The prediction results further demonstrate that L-Trp is more likely to form two hydrogen bonds with the *R*-Cu(BDA) MOF, whereas the D-Trp results show only one interaction (as shown in Figure S6). Although higher binding energies do not linearly dependent on tight binding affinity, larger values suggest larger binding capacities.[56] See Supporting Information for the details of the calculations. Analysis in conjunction with Figure S7 shows that the raw L- and D-Trp do not impact the CP photoresponse directly.

The photodetector can distinguish between enantiomers by detecting the difference in CP photocurrent enhancement of chiral SURMOFs when combined with tryptophan of D- and L-handed chirality. As shown in Figure 4b, binding of *R*-Cu(BDA) with L-Trp produced a significantly greater current signal than D-Trp in response to 330 nm RCP, while the opposite was observed for *S*-Cu(BDA) under LCP illumination. Therefore, the photocurrent changes of *R*- and *S*-Cu(BDA) based devices can be separately recorded after the addition of an unknown chiral of tryptophan, and the enantiomers can be quickly distinguished by comparing the variation of the detected signal. Furthermore, a portable circuit system with a microprocessor unit and digital signal processing chips was also prepared, as demonstrated in Figure 4c. This portable circuit is capable of recording photoresistance changes and displaying the results directly on the screen through processor data processing. For more information on the tryptophan enantiomers sensor, please refer to the Supporting Information.

In summary, we introduced a chiral, highly oriented, and monolithic MOF thin film with high optical quality that demonstrated exceptional sensitivity to the helicity of incident light. Using LPE LBL spray equipment, 2D chiral *R*- and *S*-Cu(BDA) SURMOFs oriented along the [100]-crystallographic direction have been integrated into thin-film-based CP photoelectric devices. The photoresponse when illuminated with RCP and LCP light revealed an anisotropy factor of 0.41, a competitive value compared with most reported materials and far surpassing the reported MOF CP photodetector. Additionally, this chiral SURMOF was utilized to fabricate a tryptophan enantiomer portable detector of pronounced sensitivity. This work opens up new category application fields of chiral MOFs for the realization of highly efficient CP photodetection of enantiomers.

AUTHOR INFORMATION

Corresponding Authors

Zhi-Gang Gu − *State Key Laboratory of Structural Chemistry, Fujian Institute of Research on the Structure of Matter, Chinese Academy of Sciences, 350002 Fuzhou, P. R. China;* orcid.org/0000-0001-6538-2917; Email: zggu@fjirsm.ac.cn

Christof Wöll − *Institute of Functional Interfaces (IFG), Karlsruhe Institute of Technology (KIT), 76344 Eggenstein-Leopoldshafen, Germany;* orcid.org/0000-0003-1078-3304; Email: christof.woell@kit.edu

Authors

Yi-Bo Tian − *State Key Laboratory of Structural Chemistry, Fujian Institute of Research on the Structure of Matter, Chinese Academy of Sciences, 350002 Fuzhou, P. R. China; Institute of Functional Interfaces (IFG), Karlsruhe Institute of Technology (KIT), 76344 Eggenstein-Leopoldshafen, Germany*

Koichi Tanaka − *Department of Chemistry and Materials Engineering, Kansai University, Suita, Osaka 564-8680, Japan*

Li-Mei Chang − *State Key Laboratory of Structural Chemistry, Fujian Institute of Research on the Structure of Matter, Chinese Academy of Sciences, 350002 Fuzhou, P. R. China*

Jian Zhang − *State Key Laboratory of Structural Chemistry, Fujian Institute of Research on the Structure of Matter, Chinese Academy of Sciences, 350002 Fuzhou, P. R. China;* orcid.org/0000-0003-3373-9621

Notes

The authors declare no competing financial interest.

ACKNOWLEDGMENTS

This work was supported by the National Natural Science Foundation of China (21872148) and the Youth Innovation Promotion Association of the Chinese Academy of Sciences (outstanding, Y2022081), Natural Science Foundation of Fujian Province (2022J06031), and the Fujian Science & Technology Innovation Laboratory for Optoelectronic Information of China (Grant No. 2021ZR131). C. W. acknowledges support from Deutsche Forschungsgemeinschaft (DFG, German Research Foundation) under Germany's Excellence Strategy-2082/1-390761711.

REFERENCES

(1) Chang, K.; Liu, J.; Lin, H.; Wang, N.; Zhao, K.; Zhang, A.; Jin, F.; Zhong, Y.; Hu, X.; Duan, W. Discovery of Robust in-Plane

Ferroelectricity in Atomic-Thick Snte. *Science* **2016**, *353* (6296), 274−278.
(2) Brooks, W. H.; Guida, W. C.; Daniel, K. G. The Significance of Chirality in Drug Design and Development. *Curr. Top. Med. Chem.* **2011**, *11* (7), 760−770.
(3) Lin, S.-S.; Yemelyanov, K. M.; Pugh, E.; Engheta, N. In *Polarization Enhanced Visual Surveillance Techniques*, IEEE Int. Conf. Netw. Sens. Contr. 2004, *1*, 216−221.
(4) Talmage, D.; Curran, P. Remote Sensing Using Partially Polarized Light. *Int. J. Remote Sens.* **1986**, *7* (1), 47−64.
(5) Sherson, J. F.; Krauter, H.; Olsson, R. K.; Julsgaard, B.; Hammerer, K.; Cirac, I.; Polzik, E. S. Quantum Teleportation between Light and Matter. *Nature* **2006**, *443* (7111), 557−560.
(6) Gupta, J. A.; Knobel, R.; Samarth, N.; Awschalom, D. Ultrafast Manipulation of Electron Spin Coherence. *Science* **2001**, *292* (5526), 2458−2461.
(7) Templin, R. M.; How, M. J.; Roberts, N. W.; Chiou, T.-H.; Marshall, J. Circularly Polarized Light Detection in Stomatopod Crustaceans: A Comparison of Photoreceptors and Possible Function in Six Species. *J. Exp. Biol.* **2017**, *220* (18), 3222−3230.
(8) Li, W.; Coppens, Z. J.; Besteiro, L. V.; Wang, W.; Govorov, A. O.; Valentine, J. Circularly Polarized Light Detection with Hot Electrons in Chiral Plasmonic Metamaterials. *Nat. Commun.* **2015**, *6* (1), 8379.
(9) Ishii, A.; Miyasaka, T. Direct Detection of Circular Polarized Light in Helical 1d Perovskite-Based Photodiode. *Sci. Adv.* **2020**, *6* (46), No. eabd3274.
(10) Chen, C.; Gao, L.; Gao, W.; Ge, C.; Du, X.; Li, Z.; Yang, Y.; Niu, G.; Tang, J. Circularly Polarized Light Detection Using Chiral Hybrid Perovskite. *Nat. Commun.* **2019**, *10* (1), 1927.
(11) Shang, X.; Wan, L.; Wang, L.; Gao, F.; Li, H. Emerging Materials for Circularly Polarized Light Detection. *J. Mater. Chem. C* **2022**, *10*, 2400−2410.
(12) Yang, Y.; Da Costa, R. C.; Fuchter, M. J.; Campbell, A. J. Circularly Polarized Light Detection by a Chiral Organic Semiconductor Transistor. *Nat. Photonics* **2013**, *7* (8), 634−638.
(13) Zhang, L.; Song, I.; Ahn, J.; Han, M.; Linares, M.; Surin, M.; Zhang, H.-J.; Oh, J. H.; Lin, J. π-Extended Perylene Diimide Double-Heterohelicenes as Ambipolar Organic Semiconductors for Broadband Circularly Polarized Light Detection. *Nat. Commun.* **2021**, *12* (1), 142.
(14) Wang, Z.; Gao, M.; Hao, X.; Qin, W. Helical-Chiroptical Nanowires Generated Orbital Angular Momentum for the Detection of Circularly Polarized Light. *Appl. Phys. Lett.* **2020**, *116* (5), 053301.
(15) Kim, N. Y.; Kyhm, J.; Han, H.; Kim, S. J.; Ahn, J.; Hwang, D. K.; Jang, H. W.; Ju, B.-K.; Lim, J. A. Chiroptical-Conjugated Polymer/Chiral Small Molecule Hybrid Thin Films for Circularly Polarized Light-Detecting Heterojunction Devices. *Adv. Funct. Mater.* **2019**, *29* (11), 1808668.
(16) Hao, J.; Lu, H.; Mao, L.; Chen, X.; Beard, M. C.; Blackburn, J. L. Direct Detection of Circularly Polarized Light Using Chiral Copper Chloride-Carbon Nanotube Heterostructures. *ACS Nano* **2021**, *15* (4), 7608−7617.
(17) Wang, L.; Xue, Y.; Cui, M.; Huang, Y.; Xu, H.; Qin, C.; Yang, J.; Dai, H.; Yuan, M. A Chiral Reduced-Dimension Perovskite for an Efficient Flexible Circularly Polarized Light Photodetector. *Angew. Chem., Int. Ed.* **2020**, *132* (16), 6504−6512.
(18) Long, G.; Sabatini, R.; Saidaminov, M. I.; Lakhwani, G.; Rasmita, A.; Liu, X.; Sargent, E. H.; Gao, W. Chiral-Perovskite Optoelectronics. *Nat. Rev. Mater.* **2020**, *5* (6), 423−439.
(19) Li, D.; Liu, X.; Wu, W.; Peng, Y.; Zhao, S.; Li, L.; Hong, M.; Luo, J. Chiral Lead-Free Hybrid Perovskites for Self-Powered Circularly Polarized Light Detection. *Angew. Chem., Int. Ed.* **2021**, *133* (15), 8496−8499.
(20) Guo, Z.; Richardson, J. J.; Kong, B.; Liang, K. Nanobiohybrids: Materials Approaches for Bioaugmentation. *Sci. Adv.* **2020**, *6* (12), No. eaaz0330.
(21) Liang, S.; Wu, X.-L.; Xiong, J.; Zong, M.-H.; Lou, W.-Y. Metal-Organic Frameworks as Novel Matrices for Efficient Enzyme Immobilization: An Update Review. *Coord. Chem. Rev.* **2020**, *406*, 213149.
(22) Wu, D.; Zhang, P.-F.; Yang, G.-P.; Hou, L.; Zhang, W.-Y.; Han, Y.-F.; Liu, P.; Wang, Y.-Y. Supramolecular Control of MOF Pore Properties for the Tailored Guest Adsorption/Separation Applications. *Coord. Chem. Rev.* **2021**, *434*, 213709.
(23) Sabo, M.; Henschel, A.; Fröde, H.; Klemm, E.; Kaskel, S. Solution Infiltration of Palladium into Mof-5: Synthesis, Physisorption and Catalytic Properties. *J. Mater. Chem.* **2007**, *17* (36), 3827−3832.
(24) Zhu, Y.-D.; Kang, Y.; Gu, Z.-G.; Zhang, J. Step by Step Bisacrificial Templates Growth of Bimetallic Sulfide Qds-Attached Mof Nanosheets for Nonlinear Optical Limiting. *Adv. Opt. Mater.* **2021**, *9* (7), 2002072.
(25) Cao, J.; Li, X.; Tian, H. Metal-Organic Framework (MOF)-Based Drug Delivery. *Curr. Med. Chem.* **2020**, *27* (35), 5949−5969.
(26) Arora, H.; Dong, R.; Venanzi, T.; Zscharschuch, J.; Schneider, H.; Helm, M.; Feng, X.; Cánovas, E.; Erbe, A. Demonstration of a Broadband Photodetector Based on a Two-Dimensional Metal-Organic Framework. *Adv. Mater.* **2020**, *32* (9), 1907063.
(27) Stavila, V.; Talin, A. A.; Allendorf, M. D. MOF-Based Electronic and Opto-Electronic Devices. *Chem. Soc. Rev.* **2014**, *43* (16), 5994−6010.
(28) Ren, X.; Liao, G.; Li, Z.; Qiao, H.; Zhang, Y.; Yu, X.; Wang, B.; Tan, H.; Shi, L.; Qi, X. Two-Dimensional Mof and Cof Nanosheets for Next-Generation Optoelectronic Applications. *Coord. Chem. Rev.* **2021**, *435*, 213781.
(29) Haldar, R.; Heinke, L.; Wöll, C. Advanced Photoresponsive Materials Using the Metal-Organic Framework Approach. *Adv. Mater.* **2020**, *32* (20), 1905227.
(30) Tian, Y.-B.; Vankova, N.; Weidler, P.; Kuc, A.; Heine, T.; Wöll, C.; Gu, Z.-G.; Zhang, J. Oriented Growth of In-Oxo Chain Based Metal-Porphyrin Framework Thin Film for High-Sensitive Photodetector. *Adv. Sci.* **2021**, *8* (14), 2100548.
(31) Cao, L.-A.; Yao, M.-S.; Jiang, H.-J.; Kitagawa, S.; Ye, X.-L.; Li, W.-H.; Xu, G. A Highly Oriented Conductive Mof Thin Film-Based Schottky Diode for Self-Powered Light and Gas Detection. *J. Mater. Chem. A* **2020**, *8* (18), 9085−9090.
(32) Gu, Z.-G.; Chen, S.-C.; Fu, W.-Q.; Zheng, Q.; Zhang, J. Epitaxial Growth of Mof Thin Film for Modifying the Dielectric Layer in Organic Field-Effect Transistors. *ACS Appl. Mater. Interfaces* **2017**, *9* (8), 7259−7264.
(33) Tian, Y.-B.; Wang, Y.-Y.; Chen, S.-M.; Gu, Z.-G.; Zhang, J. Epitaxial Growth of Highly Transparent Metal-Porphyrin Framework Thin Films for Efficient Bifacial Dye-Sensitized Solar Cells. *ACS Appl. Mater. Interfaces* **2020**, *12* (1), 1078−1083.
(34) Li, D.-J.; Li, Q.-h.; Gu, Z.-G.; Zhang, J. Oriented Assembly of 2d Metal-Pyridylporphyrinic Framework Films for Giant Nonlinear Optical Limiting. *Nano Lett.* **2021**, *21* (23), 10012−10018.
(35) Liu, J.; Wöll, C. Surface-Supported Metal-Organic Framework Thin Films: Fabrication Methods, Applications, and Challenges. *Chem. Soc. Rev.* **2017**, *46* (19), 5730−5770.
(36) Gu, Z.-G.; Zhang, J. Epitaxial Growth and Applications of Oriented Metal-Organic Framework Thin Films. *Coord. Chem. Rev.* **2019**, *378*, 513−532.
(37) Xiao, Y.-H.; Tian, Y.-B.; Gu, Z.-G.; Zhang, J. Surface-Coordinated Metal-Organic Framework Thin Films (Surmofs): From Fabrication to Energy Applications. *EnergyChem.* **2021**, *3* (6), 100065.
(38) Okur, S.; Qin, P.; Chandresh, A.; Li, C.; Zhang, Z.; Lemmer, U.; Heinke, L. An Enantioselective E-Nose: An Array of Nanoporous Homochiral Mof Films for Stereospecific Sensing of Chiral Odors. *Angew. Chem., Int. Ed.* **2021**, *60* (7), 3566−3571.
(39) Altaf, A.; Hassan, S.; Pejcic, B.; Baig, N.; Hussain, Z.; Sohail, M. Recent Progress in the Design, Synthesis and Applications of Chiral Metal-Organic Frameworks. *Front. Chem.* **2022**, *10*, 1014248.
(40) Li, C.; Schopmans, H.; Langer, L.; Marschner, S.; Chandresh, A.; Bürck, J.; Tsuchiya, Y.; Chihaya, A.; Wenzel, W.; Bräse, S. Twisting of Porphyrin by Assembly in a Metal-Organic Framework

Yielding Chiral Photoconducting Films for Circularly-Polarized-Light Detection. *Angew. Chem., Int. Ed.* **2023**, *62*, No. e202217377.
(41) Chen, D.-H.; Gliemann, H.; Wöll, C. Layer-by-Layer Assembly of Metal-Organic Framework Thin Films: Fabrication and Advanced Applications. *Chem. Phys. Rev.* **2023**, *4* (1), 011305.
(42) Tanaka, K.; Oda, S.; Shiro, M. A Novel Chiral Porous Metal-Organic Framework: Asymmetric Ring Opening Reaction of Epoxide with Amine in the Chiral Open Space. *Chem. Commun.* **2008**, No. 7, 820−822.
(43) Zheng, R.; Fu, Z.-H.; Deng, W.-H.; Wen, Y.; Wu, A.-Q.; Ye, X.-L.; Xu, G. The Growth Mechanism of a Conductive Mof Thin Film in Spray-Based Layer-by-Layer Liquid Phase Epitaxy. *Angew. Chem., Int. Ed.* **2022**, *61* (43), No. e202212797.
(44) Liu, J.; Lukose, B.; Shekhah, O.; Arslan, H. K.; Weidler, P.; Gliemann, H.; Bräse, S.; Grosjean, S.; Godt, A.; Feng, X. A Novel Series of Isoreticular Metal Organic Frameworks: Realizing Metastable Structures by Liquid Phase Epitaxy. *Sci. Rep.* **2012**, *2* (1), 921.
(45) Park, S. K.; Kim, J. H.; Park, S. Y. Organic 2d Optoelectronic Crystals: Charge Transport, Emerging Functions, and Their Design Perspective. *Adv. Mater.* **2018**, *30* (42), 1704759.
(46) Ji, C.; Dey, D.; Peng, Y.; Liu, X.; Li, L.; Luo, J. Ferroelectricity-Driven Self-Powered Ultraviolet Photodetection with Strong Polarization Sensitivity in a Two-Dimensional Halide Hybrid Perovskite. *Angew. Chem., Int. Ed.* **2020**, *132* (43), 19095−19099.
(47) Berthod, A. Chiral Recognition Mechanisms. *Anal. Chem.* **2006**, *78*, 2093−2099.
(48) Ranjbar, B.; Gill, P. Circular Dichroism Techniques: Biomolecular and Nanostructural Analyses-a Review. *Chem. Biol. Drug. Des.* **2009**, *74* (2), 101−120.
(49) Lin, C.-Y.; Liu, C.-C.; Chen, Y.-Y.; Chiu, K.-Y.; Wu, J.-D.; Lin, B.-L.; Wang, C.-H.; Chen, Y.-F.; Chang, S.-H.; Chang, Y.-C. Molecular Chirality Detection with Periodic Arrays of Three-Dimensional Twisted Metamaterials. *ACS Appl. Mater. Interfaces* **2021**, *13* (1), 1152−1157.
(50) Bojarska, J.; Mieczkowski, A.; Ziora, Z. M.; Skwarczynski, M.; Toth, I.; Shalash, A. O.; Parang, K.; El-Mowafi, S. A.; Mohammed, E. H.; Elnagdy, S. Cyclic Dipeptides: The Biological and Structural Landscape with Special Focus on the Anti-Cancer Proline-Based Scaffold. *Biomolecules* **2021**, *11* (10), 1515.
(51) Hassanpour, S.; Niaei, N.; Petr, J. Metal-Organic Frameworks-Based Analytical Devices for Chiral Sensing and Separations: A Review (2012−2022). *Chemosensors* **2023**, *11* (1), 29.
(52) Nan, Y.; Deng, Z.; Xi, Z.; Wu, D. Controlled Synthesis of α-Al_2O_3 Supported Ag Particles with Tuning Catalytic Performance. *J. Exp. Nanosci.* **2022**, *17* (1), 1−13.
(53) Henrich, S.; Feierberg, I.; Wang, T.; Blomberg, N.; Wade, R. C. Comparative Binding Energy Analysis for Binding Affinity and Target Selectivity Prediction. *Proteins* **2010**, *78* (1), 135−153.
(54) Ortiz, A. R.; Pisabarro, M. T.; Gago, F.; Wade, R. C. Prediction of Drug Binding Affinities by Comparative Binding Energy Analysis. *J. Med. Chem.* **1995**, *38* (14), 2681−2691.
(55) Meenambiga, S. S.; Rajagopal, K.; Durga, R. In Silico Docking Studies on the Components of Inonotus Sp., a Medicinal Mushroom against Cyclooxygenase-2 Enzyme. *Asian J. Pharm. Clin. Res.* **2015**, *8* (3), 142−145.
(56) Gallicchio, E.; Lapelosa, M.; Levy, R. M. Binding Energy Distribution Analysis Method (Bedam) for Estimation of Protein-Ligand Binding Affinities. *J. Chem. Theory Comput.* **2010**, *6* (9), 2961−2977.